

Red solitons: evidence of spatio-temporal instability in $\chi^{(2)}$ spatial-soliton dynamics

Stefano Minardi,* Giovanni Blasi, and Paolo Di Trapani
 INFN and Dipartimento di Scienze Chimiche, Fisiche e Matematiche,
 Università dell'Insubria, Via Valleggio 11, I-22100 Como, Italy

Arunas Varanavičius, Gintaras Valiulis, Audrius Beržanskis, and Algis Piskarskas
 Department of Quantum Electronics, Vilnius University,
 9 Sauletekio, building 3, LT-2040 Vilnius, Lithuania
 (Dated: September 5, 2018)

In $\chi^{(2)}$ three-wave mixing, the noise-seeded spatio-temporal modulational instability has a dramatic impact on the spatial-soliton dynamics, leading to the counterintuitive observation of a soliton with no apparent participation of the high-frequency field in the process.

Optical spatial solitons [1] are ideally monochromatic light beams whose linear diffractive spreading is compensated by a suitable non-linear phase shift. In $\chi^{(2)}$ three-wave mixing, multi-color solitary beams are sustained by energy exchange among the three waves, whose phase-velocity and wavefront-curvature mismatch give rise to an intensity-dependent phase accumulation [2]. Since their first observation in a second-harmonic generation (SHG) scheme [3], $\chi^{(2)}$ spatial solitons have been investigated in a number of different experimental conditions, *i.e.*, in up and down conversion, in bulk, waveguides and periodically-poled crystals, with gaussian and vortex-type pumps; their unique steering, addressing and switching properties have been studied in great detail for potential applications in all-optical interconnects (see reference [4] for an updated review on the topic).

With the exception of two recent experiments, where fairly short pulses and long samples were used [5, 6], all the above mentioned phenomenology has been investigated in conditions in which material chromatic dispersion was assumed to play a negligible role. However, no matter how long the input pulses are (*i.e.*, how narrow the input pulse spectra are), one should expect appreciable frequency broadening to occur, due the effect of the noise-seeded modulational instability (MI) [7]. In the spatial domain, sizeable MI impact has already been shown to cause spatial filamentation of the SHG-generated temporal soliton, for operation just above threshold [8]. By analogy, one would expect temporal pulse fragmentation to affect the spatial-soliton regime. This process is, however, difficult to detect directly since it would require ultra-high temporal resolution in single-shot acquisition mode.

In this paper we present the first evidence for the effect of noise-seeded spatio-temporal (ST) MI on $\chi^{(2)}$ spatial-soliton dynamics, which we predict to cause a temporal breakup on the 10-fs scale. We claim ST MI to be the mechanism that explains our counter-intuitive observation of a spatial soliton for which self-trapping only occurs between the low-frequency waves (*e.g.*, the signal and idler), with no apparent participation of the high-

frequency wave (*e.g.*, the pump). This is the reason we use the term “red soliton” to indicate such a process even though, strictly speaking, no solitons are formed.

Our first experiment was performed in the regime of optical parametric amplification (OPA) of the vacuum-state fluctuations, with the usual scheme assumed to lead to spatial-soliton formation [9]: a pump pulse (527 nm, 1.3 ps, 32 μ m spot FWHM) was launched on the input face of a 15 mm-long lithium triborate (LBO) crystal, operated in non-critical, type-I phase matching. For the given pump frequency (Ω_p), we tuned the signal and idler frequencies (Ω_s and Ω_i) by changing the crystal temperature. Since the chromatic dispersion (*i.e.*, the group-velocity mismatch GVM and the group-velocity dispersion GVD) experiences large changes with the tuning parameter $\Omega = \Omega_s/\Omega_p$, the setup allowed easy monitoring of the effects of dispersion on the non-linear dynamics. We should mention that here that the GVM and GVD lengths are respectively 2–4 and 10^2 – 10^3 times larger than the crystal length, across the whole tuning range.

Two different diagnostics were realized. The first is a traditional, CCD-based, beam-profile detection, which allowed recording of the fluence distribution of the pump and signal waves at the crystal output face. Note that the idler was not recorded, its photon energy being too low for the silicon detector. The second setup provided three-dimensional (*i.e.*, ST) mapping of the pump intensity profile, taken at the same crystal-output plane. The scheme is based on an ultrafast non-linear gating technique [10] realized by mixing the unknown wave packet (WP) with a 200-fs plane pulse generated by nonlinear compression of a portion of the same pump-laser pulse. The achieved temporal resolution is here of 200 fs.

Figure 1 shows the fluence profiles along the beam diameter of the pump (full line) and of the signal field (dashed line) just above threshold for soliton formation. Figure 1a refers to a crystal temperature $T = 115^\circ$ (which corresponds to $\Omega = 0.684$ and $\lambda_s = 770$ nm), close to the edge of the tuning curve; Fig. 1b refers to $T = 140^\circ$ (and thus $\Omega = 0.620$ and $\lambda_s = 850$), *i.e.* much closer to degeneracy. By looking at the result in Fig. 1a, one would rea-

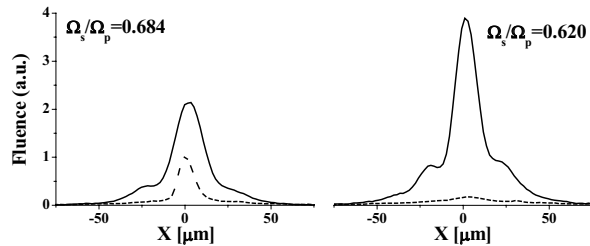


FIG. 1: Transverse fluence distribution for the output signal and pump beams for OPA excitation and two different frequency-tuning conditions (a and b), with the same pump-pulse energy, $E_p = 2.1 \mu\text{J}$.

sonably affirm that spatial solitons are formed. In fact, mutually trapped pump and signal beams of comparable peak fluence appear. The pump FWHM beam diameter ($15 \mu\text{m}$) is five times smaller than the value obtained in the linear propagation regime. In contrast, Fig. 1b contains quite a puzzling result. In fact, while the signal keeps its narrow size, the focused pump beam almost disappears into the weak background field. The background profile perfectly matches the pump-beam pedestal in Fig. 1a. Note the growth of the signal peak fluence from Fig. 1a to 1b, its value being 20 times larger than that of the pump in the second case. By taking a crystal of twice the length we obtained very similar phenomenology, the diameters of the output self-focused beams being only 30% larger than in the previous case.

A deeper insight into this rather counterintuitive observation is given by the results presented in Fig. 2 (left), where the experimental ST intensity distribution of the pump WP is plotted for two different Ω . The results show that: (i) the trailing edge of the pulse (about 200 fs) does not experience spatial trapping owing to its low input intensity. This portion accounts for the pedestal and diffracted background in Figs. 1a and 1b respectively. Note the slight temporal asymmetry of the entire ST distribution, caused by GVM. (ii) The central and leading portions, in contrast, always give rise to a spatially self-trapped profile. Its peak intensity, however, decreases dramatically as the tuning condition approaches degeneracy, which explains why the trapping seems to disappear in the time-integrated profiles. Time-resolved measurements closer to degeneracy were prevented by the low sensitivity of our CCD video trigger.

In order to provide a more accurate description of the underlying process, we performed high-resolution (4-fs step) numerical experiments by solving the three-wave parametric equations [4] within the framework of a 3D+1, ST model with radial symmetry and temporal dispersion up to third order. Figure 2 (center) shows the calculated pump profiles for conditions identical to those in Fig. 2 (left). Here the resolution of the numerical-data presen-

tation is reduced to 200 fs in order to match the resolution of the experimental diagnostic. The excellent agreement between experiment and calculation proves that the key features of the observed phenomenon are determined by the $\chi^{(2)}$ process only. Importantly, the full resolution plots, presented in Fig. 2 (right), indicate the occurrence of a temporal breakup on the 10 fs scale (the corresponding autocorrelation shows a 25 fs FWHM peak). The same structure occurs on the signal and idler waves, which appear spatially and temporally self-trapped with the pump. As to the dependence on Ω , the idler behaves in the same way as the signal wave.

Evidence for the fundamental role played by the dimensionality in the non-linear process is given by the plots in Fig. 3, where results of the experiment, of the spatio-temporal, spatial and temporal models are compared. The results indicate that while the ST model describes the experiment fairly well, both the monochromatic and plane-wave approximations completely fail to reproduce the large variation of the fluence ratio with the tuning parameter, giving an almost constant value (about unity) over the entire tuning range. This unequivocally proves that the red solitons appear as a genuine ST effect. Note that, since the temporal dynamics occurs on a time scale much shorter than that of the pulse envelope, one should not expect any appreciable effect of the input-pulse duration on the observed phenomenology. Direct numerical test with 5 ps long pulses did not produce any detectable deviation from the results shown in Fig. 3.

Our claim is that the red solitons appear as a consequence of the ST MI. In justifying this, we should first note that no theory is yet available concerning the instability of an intense, CW and focused pump beam. Therefore we must rely, in first approximation, on the predictions valid for the CW and plane-wave regime. In this case, quantum-noise parametric amplification has already been shown to appear as a branch of the MI process [11]. When the ST features of the noise are accounted for, one should not expect spatial and temporal breakup to occur as independent processes. In fact, *via* the phase-matching constraint, the parametric gain (or, equivalently, the MI) couples space and time by establishing angular dispersion and X-shaped ST spectra in the amplified modes [12]. We expect that the same key action of the gain should play a role in our experiment as well. In fact, we detected appreciable angular dispersion in the generated signal wave. Moreover, even if the temporal breakup in Fig. 2 (right) appears similar to what might be expected by a purely temporal MI, the numerical results in Fig. 3 indicate that the imbalance (*i.e.* $F_p/F_s \ll 1$) is not retrievable as long as spatial and temporal processes are considered independently.

In order to provide an explanation of the observed connection between dimensionality, imbalance and dependence on Ω we focus attention on the dramatic increase of the down-conversion bandwidth close to degeneracy,

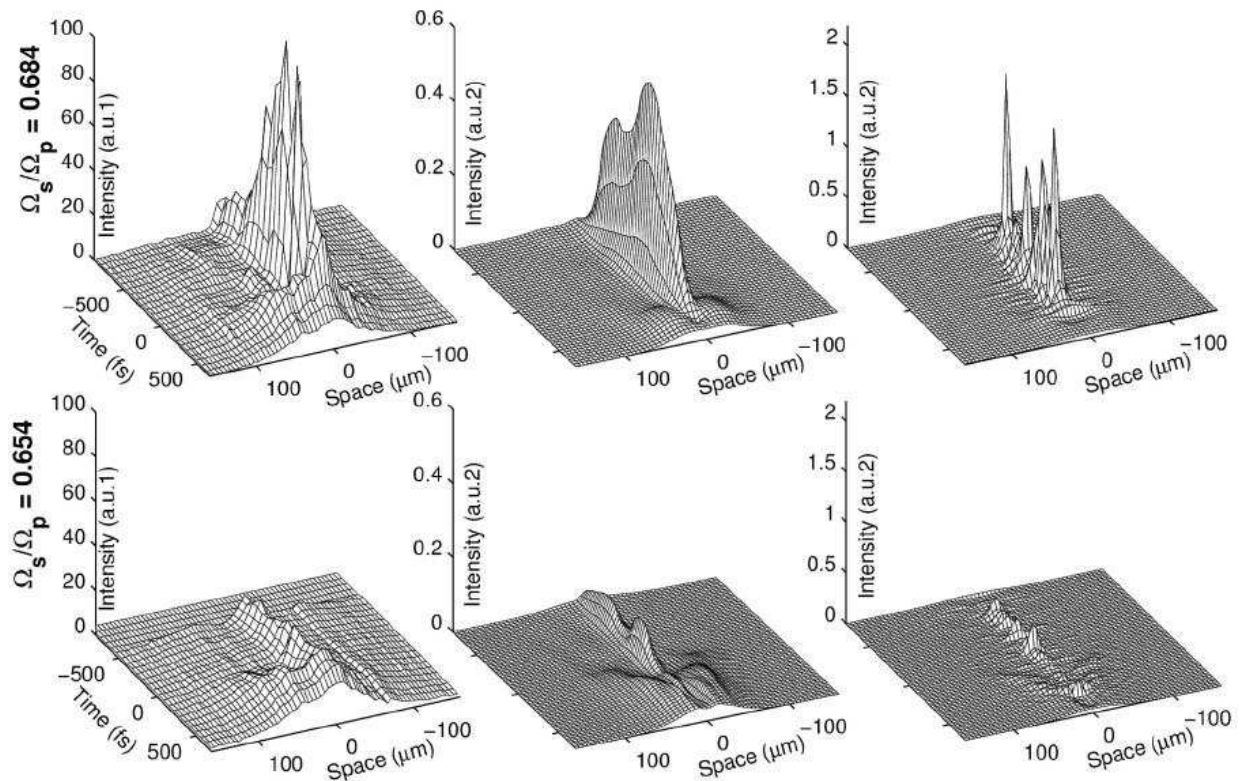


FIG. 2: Spatio-temporal intensity maps of the output pump-wave packet for OPA excitation and two different frequency-tuning conditions (top and bottom); left: experimental data; center: smoothed numerical data; right: high resolution numerical data. All data refer to the same input-pulse energy.

which should cause a down-conversion rate much larger than that for up-conversion and thus the imbalance to appear. Note that a correlation between bandwidths and imbalance must be expected as long as the signal and idler field are not correlated. In fact, in case of phase-conjugated fields, the expected drop in up-conversion efficiency induced by the filtering action of the narrow up-conversion bandwidth no longer occurs, mutual cancellation of the opposite chirps taking place without losses in the sum-frequency process [13]. This consideration explains why the 1D temporal model fails in retrieving the imbalance. In fact, a phase conjugation between signal and idler is established by the down conversion process. However, in the real 3D space, this conjugation is quenched very rapidly owing to the fast phase accumulation caused by diffraction and angular dispersion [14]. In contrast, in the plane-wave approximation, it becomes unrealistically robust, due to the weaker effect of GVD.

With the aim of verifying the generality of the process we performed a second experiment, where the spatial solitons are excited *via* SHG. The measurements, based on time-integrated detection only, were performed by focusing down to a $45\ \mu\text{m}$ spot (FWHM) a first-harmonic

(FH) pulse (1.5 ps, 1055 nm) on the input face of a 30 mm long LBO crystal, operated in non-critical, type-I phase matching. By changing the crystal temperature we tuned the phase mismatch parameter, $\Delta k = 2k_{\text{FH}} - k_{\text{SH}}$, while keeping the frequency tuning fixed at degeneracy ($\Omega = 0.5$). The results in terms of the ratio between the energy contents, $E_{\text{FH}}/E_{\text{SH}}$, at threshold (*both* FH and SH beams trapped) are presented in Fig. 4, the $\Delta k < 0$ region being limited close to phase matching by a rapid increase of the threshold with $|\Delta k|$. The few points, however, are sufficient to highlight the large discrepancy occurring for $\Delta k < 0$ between experiment and the CW-model, which predicts solitons with the opposite imbalance with respect to that measured.

The fact that the CW model fails for negative, and not for positive, phase mismatch must be related to the dominant SH content expected in this parameter region, as long as spectral broadening does not occur (see Fig. 4, full line). Due to this, the dynamics that follows the SH generation must resemble that of the OPA-excitation, where only the pump was launched at the input. To this end we mention that, for $\Delta k \leq 0$, a slight input-energy reduction caused the quenching of the trapping only in the

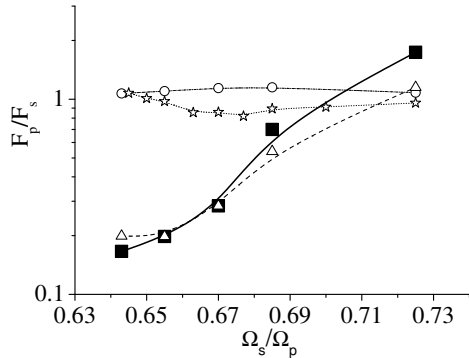


FIG. 3: Frequency-tuning dependence of the pump-to-signal (peak) fluence ratio, F_p/F_s , for OPA excitation. Squares: experimental; Triangles: 3D+1 spatio-temporal model; Circles: 2D+1 spatial model; Stars: 1D+1 temporal model. Fluences from the 3D+1 model are calculated by temporal integration. All data refer to the same input (peak) intensity.

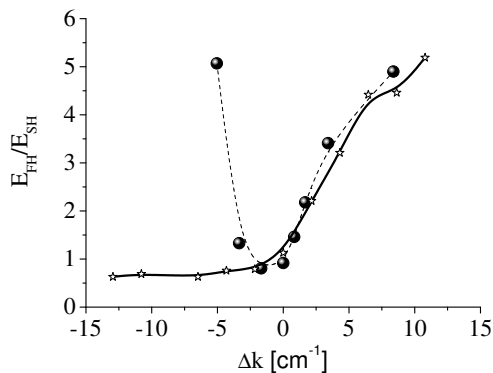


FIG. 4: Phase-mismatch dependence of the ratio between the output FH and SH energies (experimental: balls), or intensities (CW model: stars), integrated within the FWHM diameter. All data are at taken at threshold.

SH wave; this means an identical red-soliton phenomenology as described for the OPA case. In comparing the two excitation schemes, we expect that for the SHG case classical noise should also contribute to the process. As to the impact of the self-phase modulation, we mention that preliminary 3D+1 calculations performed in the absence of noise failed in retrieving the imbalance. A second peculiarity of the SHG excitation is that it leads to a true instability of the solitary regime, a spatial soliton being expected in the absence of MI. Again, since no theory has yet been developed for the MI of a bulk solitary beam, we must rely on the study of the MI of the FH+SH plane-and-monochromatic eigenmode for disclosing the mechanism of the ST interplay. Indeed, in this case too the MI has been shown to lead to the spontaneous formation of

angular dispersion, its gain curve having an X-type profile in the ST frequency domain [15].

In conclusion, we have shown that conventional, time-integrated, beam-profile measurements reveal the occurrence of a $\chi^{(2)}$ spatial soliton for which only the low-frequency signal and idler waves appear to be self-trapped. The implementation of a spatio-temporal, 3D mapping, technique has revealed that also the high-frequency pump is trapped, but with an unexpectedly weak intensity. Numerical calculations have highlighted the occurrence of a temporal break up of all the three fields on a 10fs scale. Moreover, they have shown that dispersion, diffraction and noise are all necessary elements for describing the process. Relying upon recent studies on the spatio-temporal instability of the plane and monochromatic wave in OPA and SHG, we propose an interpretation of the process as the manifestation of a noise-seeded spatio-temporal modulational instability on the $\chi^{(2)}$ spatial-soliton dynamics.

The authors wish to acknowledge the technical assistance of G. Tamosauskas and D. Mikalauskas, discussions with S. Trillo and C. Conti, and support of the MIUR (Cofin01/FIRB02), UNESCO UVO-ROSTE (875.586.2), EC CEBIOLA (ICA1-CT-2000-70027) contracts.

* Permanent address: Institute of Photonic Sciences, Jordi Girona 29, NEXUS II, E-08034 Barcelona, Spain

- [1] S. Trillo and W.E. Torruellas, eds., *Spatial Solitons* (Springer, Berlin, 2001).
- [2] G.I. Stegeman, D. Hagan and L. Torner, *Opt. and Quant. El.* **28**, 1691 (1996).
- [3] W.E. Torruellas, Z. Wang, D.J. Hagan, E.W. VanStryland, G.I. Stegeman, L. Torner and C.R. Menyuk, *Phys. Rev. Lett.* **74**, 5036 (1995).
- [4] A.V. Buryak, P. Di Trapani, D. Skryabin and S. Trillo, *Phys. Rep.* **370**, 63 (2002).
- [5] G. Valiulis, J. Kilius, O. Jedrkiewicz, A. Bramati, S. Minardi, C. Conti, S. Trillo, A. Piskarskas and P. Di Trapani, *OSA Trends in Optics and Photonics* **57**, QELS 2001 Technical Digest, postconf. edition, pap. QPD10-1.
- [6] P. Pioger, V. Couderc, L. Lefort, A. Barthelemy, F. Baronio, C. De Angelis, Y. Min, V. Quiring and W. Sohler, *Opt. Lett.* **27**, 2182 (2002).
- [7] S. Trillo and P. Ferro, *Opt. Lett.* **20**, 438 (1995).
- [8] X. Liu, K. Beckwitt and F. Wise, *Phys. Rev. Lett.* **85**, 1871 (2000).
- [9] P. Di Trapani, G. Valiulis, W. Chinaglia and A. Andreoni, *Phys. Rev. Lett.* **80**, 265 (1998).
- [10] F. Devaux and E. Lantz, *Opt. Comm.* **118**, 25 (1995).
- [11] T.A.B. Kennedy and S. Trillo, *Phys. Rev.* **A54**, 4396 (1996).
- [12] S. Orlov, A. Piskarskas and A. Stabinis, *Opt. Lett.* **27**, 2103 (2002).
- [13] F. Raoult, A.C.L. Boscheron, D. Husson, C. Sauteret, A. Modena, V. Malka, F. Dorchies and A. Migus, *Opt. Lett.* **23** 1117 (1998)
- [14] O.E. Martinez, *Opt. Commun.*, **59**, 229 (1986).

- [15] S. Trillo, C. Conti, P. Di Trapani, O. Jedrkiewicz, J. Trull, G. Valiulis and G. Bellanca, *Opt. Lett.* **27**, 1451 (2002).